Determination of the Cu 2p primary excitation spectra for Cu, Cu2O and CuO

Tougaard, Sven Mosbæk

Published in:
Surface Science

DOI:
10.1016/j.susc.2013.10.009

Publication date:
2014

Document version:
Submitted manuscript

Citation for pulished version (APA):
Tougaard, S. M. (2014). Determination of the Cu 2p primary excitation spectra for Cu, Cu2O and CuO. *Surface Science*, *620*, 17-22. https://doi.org/10.1016/j.susc.2013.10.009

Surface Science 620 (2014) 17–22

Contents lists available at ScienceDirect

Surface Science

journal homepage: www.elsevier.com/locate/susc

Determination of the Cu 2p primary excitation spectra for Cu, Cu_2O and CuO

N. Pauly [a,*], S. Tougaard [b], F. Yubero [c]

[a] Université Libre de Bruxelles, Service de Métrologie Nucléaire (CP 165/84), 50 av. F. D. Roosevelt, B-1050 Brussels, Belgium
[b] Department of Physics, Chemistry and Pharmacy, University of Southern Denmark, DK-5230 Odense M, Denmark
[c] Instituto de Ciencia de Materiales de Sevilla, Univ. Sevilla - CSIC, av. Américo Vespucio 49, E-41092 Sevilla, Spain

ARTICLE INFO

Article history:
Received 30 July 2013
Accepted 10 October 2013
Available online 17 October 2013

Keywords:
XPS, Photoelectron spectroscopy
Core-hole effect, surface effect
Copper, copper oxide

ABSTRACT

The shape and intensity of photoelectron peaks are strongly affected by extrinsic excitations due to electron transport out of the surface (including bulk and surface effects) and to intrinsic excitations due to the sudden creation of the static core hole. These effects must be included in the theoretical description of the emitted photoelectron spectra. We have calculated the effective energy-differential inelastic electron scattering cross section for XPS, including both surface and core hole effects, within the dielectric response theory by means of the QUEELS-XPS software (QUantitative analysis of Electron Energy Losses at Surfaces for XPS). The full XPS spectrum is then modeled by convoluting this energy loss cross section with the primary excitation spectrum that accounts for all effects which are part of the initial photo-excitation process, i.e. lifetime broadening, spin–orbit coupling, and multiplet splitting. The shape of this primary excitation spectrum is determined by requiring close agreement between the resulting theoretical spectrum and the experimental XPS spectrum. These calculations were performed for Cu 2p peaks of Cu, Cu_2O, and CuO. For CuO, we compare the obtained primary excitation spectra with first principle calculations performed with the CTM4XAS software (Charge Transfer Multiplet program for X-ray Absorption Spectroscopy) for the corresponding emissions and we find good quantitative agreement.

1. Introduction

X-ray photoelectron spectroscopy (XPS) is currently the most heavily used analytical techniques to obtain information about composition, electronic structure and chemical information at solid surfaces [1]. To extract quantitative information on surface atomic concentrations and on chemical bonds, it is necessary to account for the high background intensity of inelastically scattered electrons which is superimposed on the primary excited peaks. Several methods have been suggested to subtract this inelastic background from the initial spectrum. Among these, Shirley [2], Tougaard [3] and straight line [4] methods are in practice the most commonly used procedures.

The energy loss processes responsible for the background have two origins, namely the "intrinsic" and "extrinsic" excitations [5,6]. Intrinsic excitations are due to the sudden creation of the static core-hole and to the associated electric field that excites valence electrons and thus results in an energy loss by the photoelectron. Extrinsic excitations take place during the photoelectron transport process and are due to the time and space varying electric field from the moving photoelectron which also causes excitations and thereby energy losses. We note that such processes occur when the electron travels not only in the medium but also in the vacuum where the photoelectron interacts with its image charge. Thus extrinsic excitations are themselves generally separated into bulk (occurring in the medium considered as infinite) and surface processes (occurring while the electron is moving in a shallow region in the medium and in the vacuum). However, such strict separation between the various processes is not exactly valid because the effects interfere [7] and a one-step model is necessary for an accurate description.

Such one-step model based on a semi-classical dielectric response model has been proposed [7,8] and implemented in the user-friendly QUEELS-XPS software (QUantitative analysis of Electron Energy Losses at Surfaces for XPS) [9,10] which determines the energy-differential inelastic electron scattering cross-sections for XPS, K_{sc}^{XPS}, including bulk, surface and core hole effects as well as interference between these effects. This model was previously tested [8,11–13] and was shown to give a good quantitative description of the energy and angular dependence of the loss structure for various photoelectron emissions from metallic aluminium, silicon, metallic copper and iron.

In these papers, the full XPS spectra are modeled by convoluting the calculated energy loss cross section, K_{sc}^{XPS} with the primary excitation spectrum, $F(E)$ which accounts for all effects that are part of the initial photo-excitation process like life time broadening, spin–orbit coupling

* Corresponding author. Tel.: +32 2 6502083; fax: +32 2 6504534.
E-mail address: nipauly@ulb.ac.be (N. Pauly).

0039-6028/$ – see front matter © 2013 Elsevier B.V. All rights reserved.
http://dx.doi.org/10.1016/j.susc.2013.10.009

and multiplet splitting and this *F(E)* is considered as an input in the calculations. The primary goal of these previous works was to test the ability of the model to quantitatively account for observed changes in the experimental spectra when changing experimental parameters such as the excitation energy and angle of emission. It was found that this dielectric response model gave a good quantitative description. In the present work, we focus on determination of the primary excitation spectrum *F(E)* from measured photoelectron spectra.

We have thus calculated in this paper Cu 2p primary excitation spectra of Cu, Cu_2O and CuO. These metallic and oxidized forms of copper have been chosen for two reasons. First, copper is applied in a wide variety of disciplines. In its metallic form, it is always a material of choice for a variety of domestic, industrial and high-technology applications. As for copper oxides, in particular cupric (CuO) and cuprous (Cu_2O) oxide, they are of considerable interest for a multitude of applications as gas sensors, magnetic storage and recently high-T_c superconductors [14]. Second, Cu_2O and CuO display interesting and characteristic electronic structures (closed d10 shell in the case of Cu_2O and open d9 shell for CuO) due to the influence of electron-correlation effects; this results in very different Cu 2p photoemitted signals [15]. It is thus of particular interest to accurately determine the primary excitation spectra of these materials.

In the following section we describe the model used in the QUEELS-XPS software as well as the procedure followed to obtain the primary excitation spectra of the chosen transitions. Results of *F(E)* obtained within the method will then be discussed and compared, when possible, with theoretical calculations generated with the CTM4XAS software (Charge Transfer Multiplet program for X-ray Absorption Spectroscopy) [16].

2. Theoretical model

1. QUEELS formalism

The software package QUEELS-XPS [9,10] implements the dielectric response model [7] describing the interactions of electrons with semi-infinite media in terms of the dielectric properties of the bulk material and incorporates the effects of the surface, of the static core hole created during the photoionization process, and excitations in the vacuum after the photoelectron has left the surface, as well as interference between these effects. As the principles of this XPS formalism are abundantly described in the literature [6–8], we only describe here the basic elements of the model.

We consider the case of an electron-hole pair created at a depth x_0 below the surface of a semi-infinite medium characterized by its dielectric function $\varepsilon(\mathbf{k},\omega)$. The electron emission is the consequence of the photon energy absorption of a core electron. The electron travels along a straight line with velocity *v*, energy *E* and angle θ with respect to the surface normal, while the core hole is stationary with infinite lifetime. Within this model, the effective inelastic electron scattering cross section $K_{eff}^{XPS}(E,\hbar\omega,x_0,\theta)$ is defined as the average probability that the electron, excited at depth x_0, loses an energy $\hbar\omega$ per unit energy loss and per unit path length traveled inside the solid (the *XPS* in the expression of K_{eff} distinguishes this from the similar expression valid for REELS experiment where the influence of the core hole is absent [17]).

$K_{eff}^{XPS}(E,\hbar\omega,x_0,\theta)$ is then expressed in terms of the induced potential $\Phi_{ind}(\mathbf{k},\omega)$ created by the static hole and the moving electron [7]:

$$K_{eff}^{XPS}(E,\hbar\omega,x_0,\theta)=\frac{2}{(2\pi)^4 x_0\hbar^2\omega}\int_{-\infty}^{+\infty}dt\int d\mathbf{r}\rho_e(\mathbf{r},t)\times \mathrm{Re}\left[i\int d\mathbf{k}\,\mathbf{kv}\Phi_{ind}(\mathbf{k},\omega)e^{i(\mathbf{kr}-\omega t)}\right], \quad (1)$$

where $\mathbf{k}$ is the transferred momentum, $\mathbf{r}$ is the electron position, $\rho_e(\mathbf{r},t)$ is the charge density of the electron, *t* is the time (at $t=0$ photoexcitation occured), and Re[] refers to the real part of the quantity in brackets. $\Phi_{ind}(\mathbf{k},\omega)$ is obtained within the surface reflection model [18] in which the potential of a system of moving charges in a semi-infinite medium is obtained by considering two infinite pseudomedia, the medium (M) and the vacuum (V). In the pseudomedia M and V, we have to consider all charges and their images. For XPS, at $t>0$, the relevant charges are the electron $\rho_e=-e\delta(\mathbf{r}-\mathbf{x}_0-\mathbf{v}t)$, the core hole $\rho_h=e\delta(\mathbf{r}-\mathbf{x}_0)$, their images $\rho_{e^i}=-e\delta\left(\mathbf{r}+\mathbf{x}_0-\mathbf{v}^i t\right)$, $\rho_{h^i}=e\delta(\mathbf{r}+\mathbf{x}_0)$ and fictitious surface charges σ_M and σ_V introduced to satisfy the boundary conditions (in these expressions, $\mathbf{x}_0=(-x_0,0,0)$). We note that fictitious surface charges are determined by the requirement that the potentials, and the normal components of the displacement vectors in each pseudomedium must be continuous at the surface. Then, solution of Poisson's equation in Fourier space for each of the two infinite pseudomedia allows to obtain the induced potentials Φ_{ind}^M and Φ_{ind}^V. The detailed final expressions for K_{eff}^{XPS} are given in Ref. [7].

To perform this calculation, it is necessary to know the dielectric function of the medium $(\mathbf{k},\omega)$ or equivalently the energy loss function (ELF) $\mathrm{Im}\{-1/(\mathbf{k},\omega)\}$. The ELF is thus the only input in the calculations. To evaluate this latter, we consider as a model the expansion in Drude–Lindhard type oscillators [19]

$$\mathrm{Im}\left\{-\frac{1}{\varepsilon(\mathbf{k},\omega)}\right\}=\sum_{i=1}^{n}\frac{A_i\hbar\gamma_i\hbar\omega}{\left(\hbar^2\omega_{0ik}^2-\hbar^2\omega^2\right)^2+\hbar^2\gamma_i^2\hbar^2\omega^2}\theta(\hbar\omega-E_G) \quad (2)$$

with the dispersion relation:

$$\hbar\omega_{0ik}=\hbar\omega_{0i}+\alpha_i\frac{\hbar^2k^2}{2m}. \quad (3)$$

A_i, $\hbar\gamma_i$, $\hbar\omega_{0ik}$ and α_i are the strength, width, energy and dispersion of the *i*th oscillator, respectively and the step function $\theta(\hbar\omega-E_G)$ is included to describe the effect of the energy band gap E_G present in semiconductors and insulators. The parameters in the expansion are taken from Ref. [20] for the materials studied in this work, namely, Cu, Cu_2O and CuO.

In XPS experiments, electrons from a wide range of depths are sampled. This implies to perform a weighted average of K_{eff}^{XPS} over the total of all path lengths *x* [7] with the weight function $Q(E,x,\theta)$ which is the path-length distribution function for those electrons that have undergone a single inelastic collision. The result is the inelastic scattering cross-section

$$K_{sc}^{XPS}(E,\hbar\omega,\theta)=\frac{\int_0^\infty dxQ(E,x,\theta)K_{eff}^{XPS}(E,\hbar\omega,x_0,\theta)}{\int_0^\infty dxQ(E,x,\theta)}. \quad (4)$$

Within this model, K_{sc}^{XPS} includes bulk, surface and core hole effects as well as interferences between these effects.

We show in Fig. 1 the resulting effective inelastic electron scattering cross sections K_{eff}^{XPS} and the inelastic scattering cross-section K_{sc}^{XPS} obtained for photoelectrons of 320 eV emitted at an angle $\theta=15°$ with respect to the surface normal from a copper sample. For K_{eff}^{XPS}, we have chosen to show spectra from 7 emission depths, namely, 1, 2, 5, 10, 20, 40 and 65 Å. This example has been chosen because it corresponds to one of the cases studied in this paper (Cu $2p_{3/2}$ photoelectron excited by a Mg K_α X-ray source).

2. Theoretical description of the XPS spectra

An XPS spectrum can be seen as the addition of the contribution from electrons that have undergone an increasing number of energy

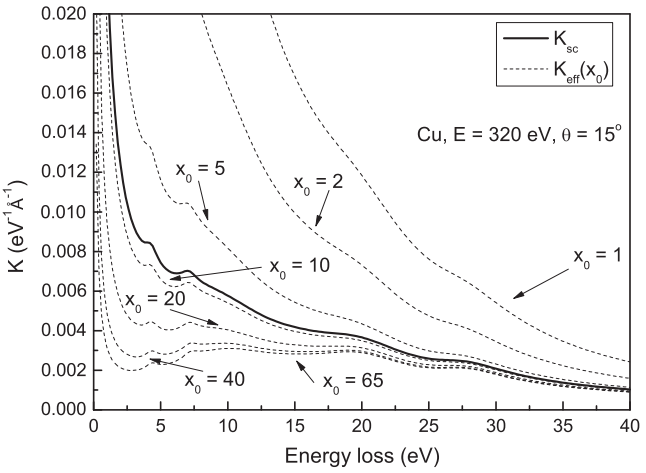

Fig. 1. Effective inelastic electron scattering cross sections $K_{eff}^{XPS}(320,\hbar\omega,x_0,15)$ of Cu for one core hole and for $x_0 = 1, 2, 5, 10, 20, 40, 65$ Å (dashed lines) and inelastic scattering cross-section $K_{sc}^{XPS}(320,\hbar\omega,15)$ (solid line).

loss processes [21] and can be written as (for a given angle of emission θ that is not written in the equation):

$$J(E)\propto F(E)+\lambda_{sc}\int_{E}^{\infty}F(E')K_{sc}^{XPS}(E_0,E'-E)dE'+\sum_{n=2}^{\infty}J_n \quad (5)$$

where $F(E)$ is the primary excited spectrum, $K_{sc}^{XPS}(E_0, E'-E)$ is the inelastic scattering cross-section as defined above for an energy loss $E'-E$ evaluated for electrons with kinetic energy E_0 and λ_{sc} is the inelastic scattering mean free path defined as

$$\lambda_{sc}(E,\theta)=\left[\int_0^{\infty}K_{sc}^{XPS}(E,\hbar\omega,\theta)d\hbar\omega\right]^{-1}. \quad (6)$$

The last term in Eq. (5) describes the contribution from multiple scattered electrons to the spectrum: $J_2(E)$ is the double scattering contribution, $J_3(E)$ the triple scattering contribution, and so on. The full spectrum can thus be modeled by repeated convolution, accounting for multiple losses.

The function $F(E)$ is the input in the calculations and is considered to take into account all quantum effects related to the initial photoexcitation process (life time broadening, spin-orbit coupling and multiplet splitting). To model $F(E)$ for the Cu 2p emission, a symmetric mixed Gaussian–Lorentzian function [4] is used:

$$F(E)=\frac{A_0 exp\left[-4(ln2)M(E-E_0)^2/\beta^2\right]}{1+4(1-M)(E-E_0)^2/\beta^2} \quad (7)$$

where A_0 is the peak height, E_0, is the peak center and β characterizes the full width at half maximum. The parameter M denotes the mixing ratio and takes the value of 1 for a pure Gaussian function and 0 for a pure Lorentzian function. The choice of the parameters in Eq. (7) is obviously limited by specific physical constraints or by previous experimental or theoretical results. The considered parameters have thus to be realistic.

3. Experimental setup

We obtain full simulated spectra by fitting results of Eq. (5) to experimental XPS spectra (Cu 2p for Cu, Cu_2O and CuO materials) with the $F(E)$ and K_{sc}^{XPS} functions as the only inputs. The experimental spectra were recorded with a non-monochromatic Mg K_α X-ray source and a hemispherical analyzer at a constant pass energy of 20 eV. The X-ray incident and exit photoelectron angles were respectively 34° and 15° with respect to the surface normal. The ambient pressure was about 10^{-10} mbar. The measured spectra are corrected for the energy dependence of the analyzer transmission, namely $E^{-0.7}$. Complete description of the experimental conditions including the procedure of production for the various samples can be found in Ref. [20].

4. Results and discussion

Fig. 2 shows results of the simulation for Cu 2p emission from a pure Cu material. Fig. 2(a) shows the determined $F(E)$ primary spectrum, the contribution from single and double scattering which are the most significant contributions as well as the sum of all multiple scattering contributions denoted total (the sum is done up to the eighth order). Also shown is the experimental spectrum. Fig. 2(b) shows $F(E)$ (zero order convolution), the sum of zero and first orders, the sum of the zero, first and second orders, the sum up to the fifth order and the total result of the simulation. The coefficients chosen to simulate $F(E)$ according to Eq. (7) are listed in Table 1. For the principal peak, we give the exact position while for the other peaks, we give the energy difference with respect to the central peak. By normalization, we have chosen an amplitude equal to one for the principal peak.

In this table and in the ones for Cu_2O and CuO targets (see below), the data corresponding to the Mg $K_{\alpha 3}$ and Mg $K_{\alpha 4}$ lines are not shown, but these lines are included in the fitting procedure for all XPS spectra. They are characterized by values given in Table 2 with as convention a negative number for a peak with a larger kinetic energy

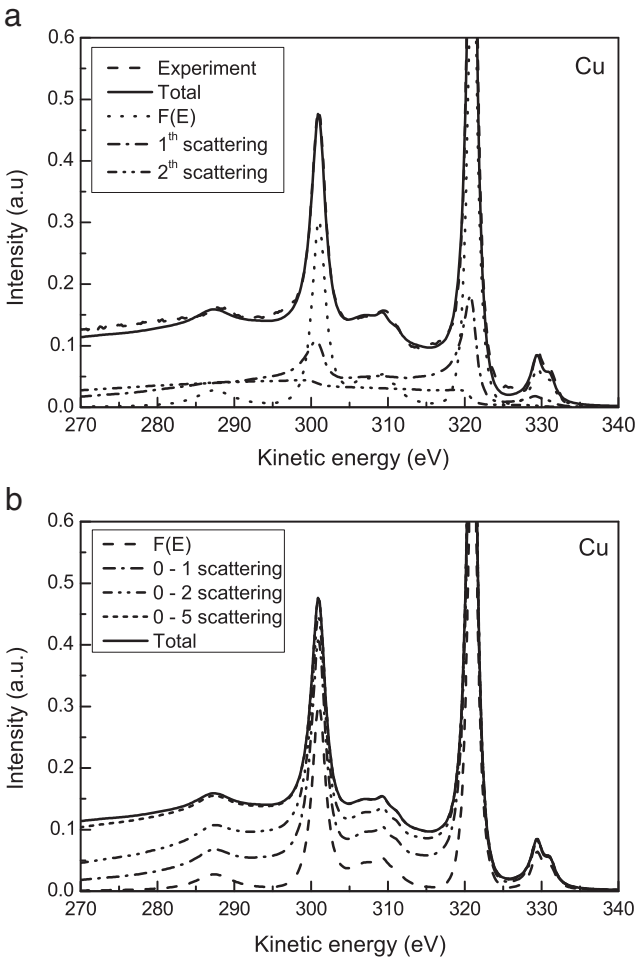

Fig. 2. Cu 2p emission from Cu: (a) total simulated spectrum (solid line), experimental spectrum (dashed line), $F(E)$ primary spectrum (dotted line), first (dash–dot) and second (dash–dot–dot) individual scattering contributions; (b) total simulated spectrum (solid line), $F(E)$ primary spectrum (dotted line), sum of zero and first orders (dash–dot), sum up to the second order (dash–dot–dot) and sum up to the fifth order (short dash).

Table 1
Parameters of the primary spectrum *F(E)* as defined by Eq. (7) for the Cu 2p emission from Cu.

Peak number	Label	E_0 (eV)	A_0	β (eV)	M
1	Main Cu 2p3/2	321.0	1.00	1.45	0.1
2	Main Cu 2p1/2	20	0.50	2.05	0.1
3	S1 to Cu 2p3/2	14.0	0.25	6.00	0.0
4	S1 to Cu 2p1/2	34.0	0.13	6.00	0.0

than the principal peak. The $K_{\alpha 3}$ and $K_{\alpha 4}$ lines are characterized in our calculations by 8.4 eVand 10.1 eV higher energy, respectively. Their intensity relative to $K_{\alpha 1,2}$ is 10% for the $K_{\alpha 3}$ line and 6% for the $K_{\alpha 4}$ line (see Table 2). These values have to be compared to the values given in Ref. [4], namely energy separations of 8.4 eV and 10.0 eV, and intensities of 9.2% and 5.1% for $K_{\alpha 3}$ and $K_{\alpha 4}$, respectively.

From Fig. 2(a), we observe that the agreement between the theoretical spectrum and the experiment is remarkably good. Obviously, it is always possible by fitting to obtain a good agreement between two curves if there is no condition on the initial input function. But this is not the case here. For each peak introduced in the source function for the 2p3/2 contribution, we have introduced its counterpart for the 2p1/2 contribution characterized by an energy exactly 20 eV smaller and with exactly half the amplitude (these pairs correspond to peaks 1/2 and 3/2 in the table). Indeed, this value of 20 eV corresponds to the energy difference between each spin–orbit contribution, namely 2p3/2 and 2p1/2, and thus to the difference between binding energies of Cu 2p3/2 and 2p1/2 [4]. Then, the factor two between the relative intensities of the doublet peaks comes from the ratio of their respective degeneracies $(2j+1)$. For *p* subshells, this factor is equal to 1/2 [4]. This approach is extensively used, in software packages like CASAXPS [22] for instance, and this justifies our choice. Moreover, we observe that the width of the peaks in each pair is similar.

The resulting *F(E)* also reveals the satellite peak S1 characterized by an energy difference (ΔE) of 14 eV (and its corresponding spin-orbit contribution with $\Delta E = 34$ eV and its intensity divided by 2). This peak S1 was clearly identified in previous works on copper and copper oxides [23,24] and is characteristic of Cu and Cu_2O while it is absent for CuO (see below).

Fig. 3 shows the "real" *F(E)* primary spectrum (shown without the $K_{\alpha 3,4}$ lines) determined from the fitting procedure, in binding energies for Cu 2p emission from a Cu target (results for Cu 2p emission from Cu_2O and CuO targets are also shown, see explanation below).

If we now examine the background structure in Fig. 2, we observe that the first scattering component shows a spike at zero energy loss. This peak is due to intrinsic excitation and clearly proves the importance of this effect in the background subtraction procedure. This contribution at zero energy loss will be much reduced for the second and higher order scattering contributions. In the model, we have assumed that the same inelastic scattering cross section K_{sc}^{XPS} can be used to account not only for the first inelastic scattering but also for the multiple inelastic scattered electrons. This is obviously a rough approximation since the multiple scattered electrons are expected to be essentially unaffected by the electron-hole interaction. However, the multiple scattered electrons are convolutions of cross sections and the main effect of these electrons is to smear out any structures and thus they do not create any new distinct features in the spectra as shown in Fig. 2.

Table 2
Parameters of the Mg $K_{\alpha 3}$ and Mg $K_{\alpha 4}$ lines.

peak number	label	E_0 (eV)	A_0	β (eV)	M
1	$K_{\alpha 3}$ to main Cu 2p3/2	−8.4	0.10	1.70	0.0
2	$K_{\alpha 3}$ to main Cu 2p1/2	11.6	0.05	2.00	0.0
3	$K_{\alpha 4}$ to main Cu 2p3/2	−10.1	0.06	1.80	0.0
4	$K_{\alpha 4}$ to main Cu 2p1/2	9.9	0.03	2.00	0.0

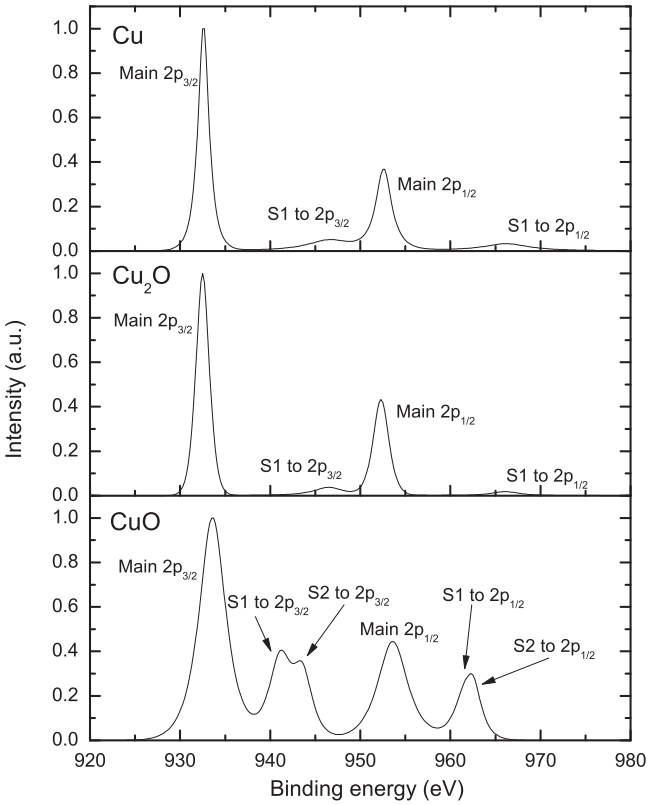

Fig. 3. *F(E)* primary spectra (without $K_{\alpha 3,4}$ lines) for Cu 2p emission from Cu, Cu_2O and CuO. Names of the lines are referred to Tables 1, 3 and 4.

Finally, we point out that in an energy region of up to about 10 eV below the main peak, the structure is well reproduced by the sum of the zero, first and second order contributions while for larger energy loss we have contributions from up to the fifth order scattering.

Fig. 4 shows equivalent results of Cu 2p emission from a Cu_2O target and Table 3, the corresponding parameters for *F(E)*. The agreement between theory and experiment is again very good. Positions of peaks of Cu_2O and pure Cu are quite similar (as shown in Ref. [23] for instance) and thus similar comments as for the Cu target apply here (except that the separation between the Cu 2p3/2 and Cu2p1/2 lines is 19.8 eV here).

Fig. 5 and Table 4 show results for the Cu 2p emission from a CuO target. A clear difference between Cu 2p characteristic peaks of CuO

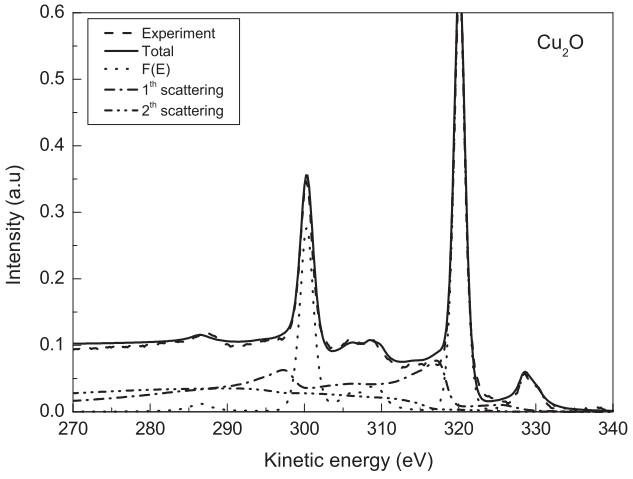

Fig. 4. Cu 2p emission from Cu_2O: total simulated spectrum (solid line), experimental spectrum (dashed line), *F(E)* primary spectrum (dotted line), first (dash–dot) and second (dash–dot–dot) individual scattering contributions.

Table 3
Parameters of the primary spectrum *F(E)* as defined by Eq. (7) for the Cu 2p emission from Cu_2O.

peak number	label	E_0 (eV)	A_0	β (eV)	M
1	Main Cu 2p3/2	321.1	1.00	1.80	0.2
2	Main Cu 2p1/2	19.8	0.50	2.10	0.2
3	S1 to Cu 2p3/2	14.0	0.12	4.00	0.0
4	S1 to Cu 2p1/2	34.0	0.06	4.00	0.0

Table 4
Parameters of the primary spectrum *F(E)* as defined by Eq. (7) for the Cu 2p emission from CuO.

peak number	label	E_0 (eV)	A_0	β (eV)	M
1	Main Cu 2p3/2	320.0	1.00	3.55	0.2
2	Main Cu 2p1/2	20.0	0.50	4.00	0.2
3	S1 to Cu 2p3/2	7.5	0.30	3.00	0.2
4	S1 to Cu 2p1/2	28.0	0.15	2.90	0.2
5	S2 to Cu 2p3/2	10.0	0.20	2.60	0.2
6	S2 to Cu 2p1/2	29.0	0.09	2.00	0.2

and Cu or Cu_2O can be seen. A pronounced double satellite peak (S1 + S2) is found at about 9 eV higher binding energy than the main Cu 2p3/2 peak in the CuO case while this satellite is absent for Cu or Cu_2O. The double peak is depicted by two peaks at 312.5 eV and 310 eV (kinetic energy), respectively. This structure is also found for the Cu 2p1/2 peak (displaced by about 20 eV). The presence of these satellites is explained in a molecular orbital description by a charge transfer mechanism [15]. Indeed, CuO has an open d shell (3d9) and then exhibits a mixture of 3d9 and 3d10L configurations (where L represents an O 2p ligand hole). After the core hole creation, two final states are thus possible: in one of them, one electron is transferred from the ligand into the Cu 3d level, corresponding to the main line with a final configuration given by c3d10L (c denotes a hole in the core level) and in the other possible final state, no charge transfer occurs and the system keeps a c3d9 configuration (assigned to the satellite line). We note in Table 4 that all lines for CuO are broadened compared to Cu and Cu_2O. For the main peaks this is consistent with the theoretical assumption that the system can end up in several final states c3d10L depending on the energy of the hole L and for the satellites, it is the result of multiplet splitting in the final state: eight final states for (2p3/2)3d9 and four for (2p1/2)3d9 corresponding to total angular momentum in J–J coupling. We have not considered in our fitting procedure this high level of multiplicity because of the too large number of fitting possibilities. We note that the previous "rules" concerning the energy separation of 20 eV between each spin–orbit contribution and the factor two between the corresponding intensities may not be strictly true since the multiplet splitting for 2p1/2 need not be the same as for 2p3/2. However we approximately kept this constraint for simplicity.

Again, our fitting procedure also gives a very good agreement with the experimental spectrum. But for this peak it is also possible to compare our primary excitation spectrum with theoretical calculations performed within the charge transfer multiplet model implemented in the software CTM4XAS (Charge Transfer Multiplet program for X-ray Absorption Spectroscopy) [16]. Among other things, CTM4XAS is intended to calculate photoemission spectra for transition metal systems, including two configurations, 3dn and 3d(n + 1)L. For XPS especially, the software is capable of calculating 1 s, 2 s, 3 s, 2p and 3p spectra. Unfortunately, for Cu, only the Cu2 + and Cu3 + configurations are available in the database provided with CTM4XAS. This allows calculations for only CuO and not for the other materials considered in the present work. We emphasize that the goal of this work was not to determine the best parameters to be used in CTM4XAS but to compare results previously obtained by other groups with our own primary excitation spectrum.

We have thus considered without any change the most recent parameters suggested in Ref. [25] that are hybridization potential with D_{4h} local symmetry around the Cu ion ($U_{b1} = 2.00$ eV, $U_{a1} = U_{b1}/\sqrt{3}$, $U_{b2} = U_{b1}/2$ and $U_e = \sqrt{2}U_{b2}$), charge transfer energy from the center of the valence band to the 3d levels $\Delta = 1.46$ eV, and strength of the

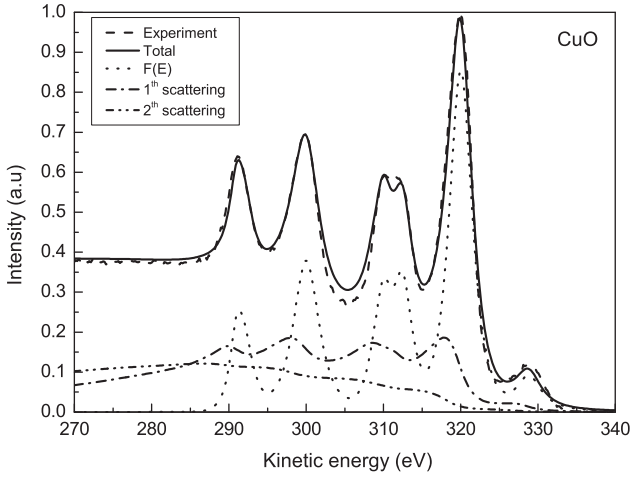

Fig. 5. Cu 2p emission from CuO: total simulated spectrum (solid line), experimental spectrum (dashed line), *F(E)* primary spectrum (dotted line), first (dash–dot) and second (dash–dot–dot) individual scattering contributions.

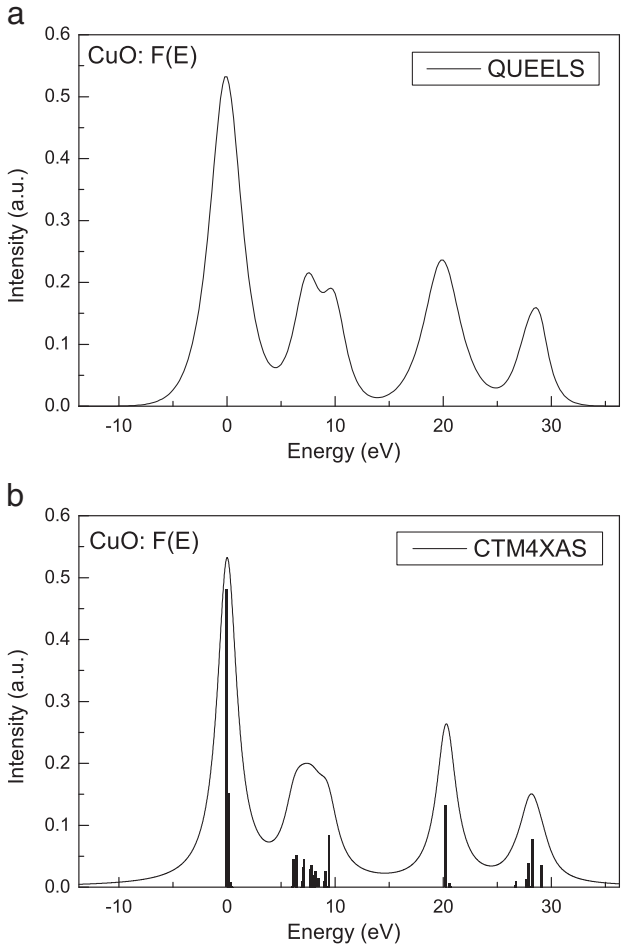

Fig. 6. *F(E)* primary spectra (without $K_{\alpha 3,4}$ lines) for Cu 2p emission (CuO target) obtained from (a) QUEELS (b) CTM4XAS (including sticks) in relative energy scale.

core hole potential acting on the 3d electrons $U_{pd} = 8.00$ eV (more details in ref. [16] and references therein). A comparison between our *F(E)* spectrum with the theoretical spectrum obtained from CTM4XAS with a broadening of 1 eV is shown in Fig. 6. The agreement between the two results is quite good.

5. Conclusion

In this work, we have determined the Cu 2p primary excitation spectra of Cu, Cu_2O and CuO. This was done by first calculating the effective differential inelastic scattering cross section for XPS within the semiclassical dielectric response model which includes the effects of the core hole and effects of the surface as well as interference effects. This cross section was convoluted with a model primary spectrum which was varied until a good agreement with the experimental XPS was obtained. For all materials it was possible to obtain a good agreement over a large energy range using realistic constraints of the fitting parameters.

Moreover, we compare our result for CuO 2p emission with theoretical calculations generated with the CTM4XAS software using input data that were previously published and again a good quantitative agreement is found.

We thus show that our model allows to determine the primary excitation spectrum by subtracting a background calculated from physical arguments including extrinsic and intrinsic energy loss contributions.

References

[1] In: D. Briggs, J.T. Grant (Eds.), Surface Analysis by Auger and X-Ray Photoelectron Spectroscopy, IM-Publications, Chichester, 2003.
[2] D.A. Shirley, Phys. Rev. B 5 (1972) 4709.
[3] S. Tougaard, Surf. Sci. 216 (1989) 343.
[4] In: D. Briggs, M.P. Seah (Eds.), Vol. 1, Wiley, Chichester, 1990.
[5] P.H. Citrin, G.K. Wertheim, Y. Baer, Phys. Rev. B 16 (1977) 4256.
[6] S. Tougaard, J. Electron Spectrosc. Relat. Phenom. 178 (2010) 128.
[7] A.C. Simonsen, F. Yubero, S. Tougaard, Phys. Rev. B 56 (1997) 1612.
[8] F. Yubero, S. Tougaard, Phys. Rev. B 71 (2005) 045414.
[9] S. Tougaard, F. Yubero, Surf. Interface Anal. 36 (2004) 824 (information on the software is available at www.quases.com).
[10] S. Tougaard, F. Yubero, Surf. Interface Anal. 44 (2012) 1114.
[11] Z. Berényi, L. Kövér, S. Tougaard, F. Yubero, J. Tóth, I. Cserny, D. Varga, J. Electron Spectrosc. Relat. Phenom. 135 (2004) 177.
[12] F. Yubero, L. Kövér, W. Drube, Th. Eickhoff, S. Tougaard, Surf. Sci. 592 (2005) 1.
[13] F. Yubero, S. Tougaard, J. Electron Spectrosc. Relat. Phenom. 185 (2012) 552.
[14] L. Debbichi, M.C. Marco de Lucas, J.F. Pierson, P. Krüger, J. Phys. Chem. C 116 (2012) 10232.
[15] J. Ghijsen, L.H. Tjeng, J. van Elp, H. Eskes, J. Westerink, G.A. Sawatzky, Phys. Rev. B 38 (1988) 11322.
[16] E. Stavitski, F.M.F. de Groot, Micron 41 (2010) 687.
[17] F. Yubero, J.M. Sanz, B. Ramskov, S. Tougaard, Phys. Rev. B 53 (1996) 9719.
[18] J.L. Gervasoni, N.R. Arista, Surf. Sci. 260 (1992) 329.
[19] R.H. Ritchie, A. Howie, Philos. Mag. 36 (1977) 463.
[20] D. Tahir, S. Tougaard, J. Phys. Condens. Matter 24 (2012) 175002.
[21] S. Tougaard, P. Sigmund, Phys. Rev. B 25 (1982) 4452.
[22] N. Fairley, CasaXPS Version 2.3.15: Software package for data processing, http://www.casaxps.com.
[23] S.Y. Lee, N. Mettlach, N. Nguyen, Y.M. Sun, J.M. White, Appl. Surf. Sci. 206 (2003) 102.
[24] J. Zhang, Y. Wang, P. Cheng, Y.L. Yao, J. Appl. Phys. 99 (2006) 064902.
[25] K. Okada, A. Kotani, J. Electron Spectrosc. Relat. Phenom. 52 (1990) 313.